Predicting evolutionary site variability from structure in viral proteins: buriedness, flexibility, and design

Amir Shahmoradi,[1,2] Dariya K. Sydykova,[2] Stephanie J. Spielman,[2]
Eleisha L. Jackson,[2] Eric T. Dawson,[2] Austin G. Meyer,[2] Claus O. Wilke[2]

[1] Department of Physics, The University of Texas at Austin, TX, 78712
[2] Department of Integrative Biology, Center for Computational Biology and Bioinformatics, and
Institute for Cellular and Molecular Biology, The University of Texas at Austin, TX, 78712

Abstract

Several recent works have shown that site-specific evolutionary variation in proteins can be predicted from protein structure. Most prominently, sites that are buried and/or have many contacts with other sites in a structure evolve more slowly than surface sites with few contacts. Here, we present a comprehensive study of numerous different structural properties that may constrain sequence variation, including measures of buriedness (relative solvent accessibility, contact number), measures of structural fluctuations (B factors, root-mean-square fluctuations, variation in dihedral angles), and variability in designed structures. Structural fluctuation measures were obtained from molecular dynamics simulations performed on 9 non-homologous viral protein structures, and from variation in homologous variants of these proteins where available. Variability in designed structures was obtained from flexible-backbone design via Rosetta. We found that most of the structural properties correlate with site variation in the majority of structures, though the correlations are generally weak (correlation coefficients of 0.1 to 0.4). We further found that measures of buriedness tend to be better predictors of evolutionary variation than measures of structural fluctuations. Variability in designed structures was a weaker predictor of evolutionary variability than both measures of buriedness and measures of fluctuations. We conclude that simple measures of buriedness are better predictors of evolutionary variation than more complicated predictors obtained from dynamic simulations, ensembles of homologous structures, or computational protein design.

Introduction

Patterns of sequence variation in protein-coding genes are shaped by the biophysical structure and function of the expressed proteins (Wilke and Drummond, 2010; Marsh and Teichmann, 2014). As the most basic reflection of this relationship, buried residues in proteins tend to be more evolutionarily conserved than exposed residues (Overington et al., 1992; Goldman et al., 1998; Mirny and Shakhnovich, 1999; Dean et al., 2002). More specifically, when evolutionary variation is plotted as a function of Relative Solvent Accessibility (RSA, a measure of residue

buriedness), it falls, on average, onto a straight line (Franzosa and Xia, 2009; Ramsey et al., 2011; Franzosa and Xia, 2012; Scherrer et al., 2012). We need to emphasize, however, that this relationship represents an average over many sites and many proteins. At the level of individual sites in individual proteins, RSA is often only weakly correlated with evolutionary variation (Meyer and Wilke, 2013; Meyer et al., 2013; Yeh et al., 2014).

Measures of residue buriedness other than RSA have also been shown to correlate with sequence variability, for example residue contact number (Liao et al., 2005; Franzosa and Xia, 2009; Yeh et al., 2014). Some have argued that contact number serves as a better predictor of evolutionary variation than RSA (Yeh et al., 2014). Because contact number may be a proxy of residue and site-specific backbone flexibility (Halle, 2002), one may also expect to observe a positive trend between local structural flexibility and sequence variability (Yeh et al., 2014). Indeed, several authors have argued for the potential role of protein dynamics in sequence variability (Liu and Bahar, 2012; Nevin Gerek et al., 2013; Marsh and Teichmann, 2014). However, a recent paper argued against the flexibility model, on the grounds that it should introduce certain non-linearities that are not observed in the data (Huang et al., 2014).

Measures of residue buriedness or packing density can be calculated in a straightforward manner from individual crystal structures. By contrast, measures of structural flexibility, either at the side-chain or the backbone level, are more difficult to obtain. Ideally, one would want to observe physiologically relevant structural fluctuations *in vivo*. An approximate measure of such fluctuations could be the variations observed in NMR ensembles. Further, the thermal motion of atoms in a crystal are recorded in B factors, which are available for every atom in every PDB structure. However, it is unclear how accurately B factors reflect structural fluctuations of a protein in solution. One can also attempt to assess physiologic fluctuations by aligning multiple homologous PDB structures. Alternatively, one can consider a simulation approach, either using coarse-grained modeling, e.g. via Elastic Network Models (Sanejouand, 2013), or using atom-level modeling, e.g. via molecular dynamics (MD) (Karplus and McCammon, 2002). It is currently not well understood which (if any) of these measures of structural fluctuations are predictive of evolutionary variation, and to what extent they provide distinct insight into the evolutionary process.

Here, we provide a comprehensive analysis of the extent to which numerous different structural quantities predict evolutionary variation. As structural predictors, we include both measures of buriedness, such as RSA and contact number, and measures of structural fluctuations, including B factors, several measures of backbone and side-chain variability obtained from MD simulations, and backbone variability obtained from alignments of homologous crystal structures. We also include site variability predicted from computational protein design. On a set of 9 viral proteins, we find that measures of buriedness generally perform better at predicting evolutionary site variation than either measures of structural fluctuations or computational protein design. Among the measures of structural fluctuations, measures of side-chain variability seem to perform better than measures of backbone variability, possibly because the former are more closely correlated with residue buriedness. Finally, site variability predicted from computational protein design performs worse than the best-performing measures of structural fluctuations.

Materials and Methods

Sequence data, alignments, and evolutionary rates

All viral sequences except influenza sequences were retrieved from `http://hfv.lanl.gov/components/sequence/HCV/search/searchi.html`. The sequences were truncated to the desired genomic region but not in any other way restricted. Influenza sequences were downloaded from `http://www.fludb.org/brc/home.spg?decorator=influenza`. We only considered human influenza A, H1N1, excluding H1N1 sequences derived from the 2009 Swine Flu outbreak. We only used sequences from after 1998 but did not place any geographic restrictions.

For all viral sequences, we removed any sequence that was not in reading frame, any sequence which was shorter than 80% of the longest sequence for a given viral protein (so as to remove all partial sequences), and any sequence containing any ambiguous characters. Alignments were constructed using amino-acid sequences with MAFFT (Katoh et al., 2002, 2005), specifying the `--auto` flag to select the optimal algorithm for the given data set, and then back-translated to a codon alignment using the original nucleotide sequence data.

To assess site-specific sequence variability in amino-acid alignments, we calculated the Shannon entropy (H_i) at each alignment column i:

$$H_i = -\sum_j P_{ij} \ln P_{ij}, \tag{1}$$

where P_{ij} is relative frequency of amino acid j at position i in the alignment.

For each alignment, we also calculated evolutionary rates, as described (Spielman and Wilke, 2013). In brief, we generated a phylogeny for each codon alignment in RAxML (Stamatakis, 2006) using the GTRGAMMA model. Using the codon alignment and phylogeny, we inferred evolutionary rates with a Random Effects Likelihood (REL) model, using the HyPhy software (Kosakovsky Pond et al., 2005). The REL model was a variant of the GY94 evolutionary model (Goldman and Yang, 1994) with five ω rate categories as free parameters. We employed an Empirical Bayes approach (Yang, 2000) to infer ω values for each position in the alignment. These ω values represent the evolutionary-rate ratio dN/dS at each site.

Protein crystal structures

A total of 9 viral protein structures were selected for analysis, as tabulated in Table 1. Sites in the PDB structures were mapped to sites in the viral sequence alignments via a custom-built python script that creates a consensus map between a PDB sequence and all sequences in an alignment.

For each of the viral proteins, homologous structures were identified using the `blast.pdb` function of the R package Bio3D (Grant et al., 2006). BLAST hits were retained if they had $\geq 35\%$ sequence identity and $\geq 90\%$ alignment length. Among the retained hits, we subsequently identified sets of homologous structures with unique sequences and with mutual pairwise sequence divergences of $\geq 2\%$, $\geq 5\%$, and $\geq 10\%$.

3

Measures of buriedness and of structural flexibility

As measures of residue buriedness, we calculated Relative Solvent Accessibility (RSA), contact number (CN), and weighted contact number (WCN). To calculate RSA, we first calculated the Accessible Surface Area (ASA) for each residue in each protein, using the DSSP software (Kabsch and Sander, 1983). We then normalized ASA values by the theoretical maximum ASA of each residue (Tien et al., 2013) to obtain RSA. We calculated CN for each residue as the total number of $C\alpha$ atoms surrounding the $C\alpha$ atom of the focal residue within a spherical neighborhood of a predefined radius r_0. Following Yeh et al. (2014), we used $r_0 = 13\mathring{A}$. We calculated WCN as the total number of surrounding $C\alpha$ atoms for each focal residue, weighted by the inverse square separation between the $C\alpha$ atoms of the focal residue and the contacting residue, respectively (Shih et al., 2012).

In most analyses, we actually used the inverse of CN and/or WCN, iCN = 1/CN and iWCN = 1/WCN. Note that for Spearman correlations, which we use throughout here, replacing a variable by its inverse changes the sign of the correlation coefficient but not the magnitude.

As measures of structural variability, we considered RMSF, variability in backbone and side-chain dihedral angles, and B factors. We calculated RMSF for backbone $C\alpha$ atoms based on both MD trajectories and homologous structures. For MD trajectories, we calculated RMSF as

$$\text{RMSF}_j = \Big[\sum_i \big(\mathbf{r}_i^{(j)} - \mathbf{r}_0^{(j)}\big)^2 \Big]^{1/2} \tag{2}$$

where RMSF_j is the root-mean-square fluctuation at site j, $\mathbf{r}_i^{(j)}$ is the position of the $C\alpha$ atom of residue j at MD frame i, and $\mathbf{r}_0^{(j)}$ is the position of the $C\alpha$ atom of residue j in the original crystal structure.

To calculate RMSF from homologous structures, we first aligned the structures using the Bio3D package (Grant et al., 2006), and then we calculated

$$\text{RMSF}_j = \Big[\sum_i w_i \big(\mathbf{r}_i^{(j)} - \langle \mathbf{r}^{(j)} \rangle\big)^2 \Big]^{1/2}, \tag{3}$$

where $\mathbf{r}_i^{(j)}$ now stands for the position of the $C\alpha$ atom of residue j in structure i, $\langle \mathbf{r}^{(j)} \rangle$ is the mean position of that $C\alpha$ atom over all aligned structures, and w_i is a weight to correct for potential phylogenetic relationship among the aligned structures. The weights w_i were calculated using BranchManager (Stone and Sidow, 2007), based on phylogenies built with RAxML as before.

To assess variability in backbone and side-chain dihedral angles, we calculated $\text{Var}(\phi)$, $\text{Var}(\psi)$, and $\text{Var}(\chi_1)$. The variance of a dihedral angle was defined according to the most common definition in directional statistics: First, a unit vector $\mathbf{x}_i$ is assigned to each dihedral angle α_i in the sample. The unit vector is defined as $\mathbf{x}_i = (\cos(\alpha_i), \sin(\alpha_i))$. The variance of the dihedral angle is then defined as

$$\text{Var}(\alpha) = 1 - ||\langle \mathbf{x} \rangle||, \tag{4}$$

where $||\langle \mathbf{x} \rangle||$ represents the length of the mean $\langle \mathbf{x} \rangle$, calculated as $\langle \mathbf{x} \rangle = \sum_i \mathbf{x}_i/n$. Here, n is the sample size. The variance of a dihedral angle is, by definition, a real number in the range

$[0, 1]$, with $\text{Var}(\alpha) = 0$ corresponding to the minimum variability of the dihedral angle and $\text{Var}(\alpha) = 1$ to the maximum, respectively (Berens, 2009). Since the χ_1 angle is undefined for Ala and Gly we excluded all sides with these residues in analyses involving χ_1.

B factors were extracted from the crystal structures. We only considered the B factors of the Cα atom of each residue.

Molecular Dynamics Simulations

Molecular dynamics (MD) simulations were carried out using the GPU implementation of the *Amber12* simulation package (Salomon-Ferrer et al., 2013) with the most recent release of the Amber fixed-charge force field (ff12SB; c.f., AmberTools13 Manual). Prior to MD production runs, all PDB structures were first energy minimized using the steepest descent method for 1000 steps, followed by conjugate gradient for another 1000 steps. Then, the structures were constantly heated from 0K to 300K for 0.1ns, followed by 0.1ns constant pressure simulations with positional harmonic restraints on all atoms to avoid instabilities during the equilibration process. The systems were then equilibrated for another 5ns without positional restraints, each followed by 15ns of production simulations for subsequent post-processing and analyses. All equilibration and production simulations were run using the SHAKE algorithm (Ryckaert et al., 1977). Langevin dynamics were used for temperature control.

Sequence Entropy from Designed Proteins

Designed entropy was calculated as described (Jackson et al., 2013). In brief, proteins were designed using RosettaDesign (Version 39284) (Leaver-Fay et al., 2011) using a flexible backbone approach. This was done for all PDB structures in Table 1 as initial template structures. For each template, we created a backbone ensemble using the Backrub method (Smith and Kortemme, 2008). The temperature parameter in Backrub was set to 0.6, allowing for an intermediate amount of flexibility. For each of the 9 template structures we designed 100 proteins.

Availability of data and methods

All details of simulations, input/output files and scripts for subsequent analyses are available to view or download at `https://github.com/clauswilke/structural_prediction_of_ER`.

Results

Data set and structural variables considered

Our goal in this work is to determine which structural properties best predict amino-acid variability at individual sites in proteins. To this end, we selected 9 viral proteins for which we had both high-quality crystal structures and abundant sequences to assess evolutionary

variability (Table 1). We quantified evolutionary variability in two ways, by calculating entropies for each alignment column (sequence entropy) and by calculating the evolutionary-rate ratio $\omega = dN/dS$ (see Methods for details). Throughout this paper, we primarily report results obtained for sequence entropy. Results for ω are largely comparable, with some specific caveats detailed below.

As predictors of evolutionary variability, we considered two broad classes of structural properties, residue buriedness and residue flexibility. Measures of buriedness quantify the extent to which a residue is protected from solvent. A commonly used measure of buriedness is solvent-accessible surface area (ASA) or its normalized variant relative solvent accessibility (RSA). Here we considered RSA, since it can be compared among residues of different sizes. We also considered contact number (CN) and weighted contact number (WCN). Both of these quantities assess the number of other residues a focal residue contacts. CN simply counts the number of contacts within a sphere of a given radius around the α-carbon of the focal residue. WCN weights contacts by the distance between the two residues. Note that residue buriedness decreases as RSA increases, but it increases with increasing CN or WCN. To avoid this difference in directionality, in most analyses we replaced CN and WCN with their inverse, iCN = 1/CN and iWCN = 1/WCN. Because nearly all analyses we carried out were non-parametric and only depended on the rank order of the variables, this substitution only changed the sign of correlations but not the magnitude.

Measures of flexibility assess the extent to which a residue fluctuates in space as a protein undergoes thermodynamic fluctuations in solution. There are different ways to quantify these fluctuations. First, we can measure the root mean-square deviation of the Cα atom over time. This quantity is commonly called RMSF. Second, we can consider B factors, which measure the spatial localization of individual atoms in a protein crystal. Third, we can measure the variability in side-chain or backbone dihedral angles, such as Var(χ_1), Var(ϕ), or Var(ψ). Here, we considered all these measures of structural variability.

To calculate measures of flexibility, we generated molecular-dynamics (MD) trajectories for all crystal structures in Table 1. In all cases, we equilibrated the structure and then simulated 15ns of chemical time (see Methods). We recorded snapshots of the simulated structure every 10ps. From these snapshots, for each residue we calculated RMSF as well as the variability in dihedral and side-chain angles. We also calculated time-averaged values of the three measures of buriedness RSA, CN, and WCN. We refer to these time-averaged values as MD RSA, MD CN, and MD WCN, respectively.

Structural buriedness vs. structural flexibility as predictors of evolutionary variation

We first compared a subset of variables among the measures of buriedness and measures of fluctuations in their explanatory power for sequence variation. Figure 1 shows the Spearman correlation between sequence entropy and each of the quantities RSA, iWCN, Var(χ_1), RMSF, and B factor, for each protein. Significant correlations ($P < 0.05$) are shown with filled symbols, and non-significant correlations are shown with empty symbols ($P \geq 0.05$). In this figure, several patterns emerge. First, all correlations are generally positive and significant. The main exception is the RNA binding domain of Marburg virus, PDB ID 4GHA,

which mostly shows no correlation but shows a negative correlation between sequence entropy and the variability in the χ_1 angle. Second, correlations are generally weak. No correlation coefficient exceeds 0.4. Third, on average the correlation strength decreases as we move from left to right in the figure. The two measures of buriedness, RSA and iWCN, show the strongest correlations. Their correlations are on average $\rho = 0.23$ and $\rho = 0.22$, respectively. The three fluctuation measures Var(χ_1), RMSF, and B factor exhibit weaker correlations, on average $\rho = 0.14$, $\rho = 0.11$, and $\rho = 0.12$, respectively.

We next analyzed structural fluctuations more carefully, by comparing the correlations of entropy with six different measures of local structural flexibility. We considered variations in the backbone and side-chain dihedral angles (ϕ, ψ, and χ_1), B factors, RMSF obtained from MD simulations, and RMSF obtained from crystal structures. For the latter quantity, we aligned homologous structures with distinct sequences, obtained from the PDB (see Methods and Table 2 for details). The correlation strengths of these quantities with entropy are shown in Figure 2. We found that the variation in backbone dihedral angles, Var(ϕ) and Var(ψ), explained the least variation in sequence entropy, while the variation in the side-chain dihedral angle Var(χ_1) explained, on average, more variation in sequence entropy than any other measure of structural flexibility. B factors and the two measures of RMSF explained on average approximately the same amount of variation in entropy, even though the results for individual proteins were somewhat discordant (see also next sub-section).

MD time-averages vs. crystal-structure snapshots

For most analyses discussed so far, except analyses involving B factors or crystal RMSF, we averaged structural quantities over MD trajectories comprising 15ns of chemical time. This is not conventional practice for quantities such as RSA or contact numbers. Instead, most authors simply obtain these quantities from individual crystal structures. We therefore asked whether MD averages differed in any meaningful way from estimates obtained from crystal structures, and whether estimates from MD and from crystal structures different in their predictive power for sequence variability.

We found that RSA, CN, and WCN from crystal structures were highly correlated with their averages over MD trajectories, for all protein structures we examined (Spearman correlation coefficients of > 0.9 in all cases, Table 3). Further, when we correlated these quantities with sequence entropy, we found that the correlation coefficients we obtained for each protein were virtually identical (Figure 3A-C). Thus, in terms of predicting evolutionary variation, RSA and contact numbers obtained from the static structures performed as well as their dynamic equivalents averaged over short time scales.

By contrast, we found more variation when we considered backbone flexibility as measured by root mean fluctuations (RMSF). RMSF cannot be obtained from a single crystal structure, but we can calculate it from an alignment of multiple crystal structures were available. When we compared RMSF from MD to RMSF from crystal structures, we found that they were sometimes quite different, with correlation coefficients ranging from 0.218 to 0.723 (Table 3). Consequently, for the two proteins for which MD RMSF was the least correlated with crystal-structure RMSF (hepatitis C protease and Rift Valley fever nucleoprotein), the strength of the correlation between site entropy and RMSF depended substantially on whether RMSF was obtained from MD or from crystal structures (Figures 2 and 3D).

To further investigate the relationship between backbone fluctuations and sequence variability, we also compared the RMSF correlations to the correlations between sequence entropy and B factors. Again, we found that these correlations were generally different from the ones found for either the MD RMSF or the crystal structure RMSF (Figure 4). Thus, B factors, MD RMSF, and crystal RMSF, though all measures of backbone fluctuations, contained distinct information about sequence variability in our data set.

Sequence entropy vs. evolutionary-rate ratio ω

In the previous subsections, we have used sequence entropy as a measure of amino-acid variability at individual sites. While sequence entropy is a simple and straightforward measure of site variability, it has two potential drawbacks: First, entropy doesn't correct for the phylogenetic relationship of sequences in the alignment, and hence it can be biased if some parts of the phylogeny are more densely sampled than others. Second, entropy does not take into account the actual substitution process. As a result, a single substitution near the root of the tree can result in a comparable entropy to a sequence of substitutions toggling back and forth between two amino acids.

To consider an alternative quantity of sequence variability that doesn't suffer from either of these drawbacks, we calculated the evolutionary-rate ratio $\omega = dN/dS$ for all proteins at all sites, and repeated all analyses with ω instead of entropy. We found that all results generally carried over, but the correlations tended to be somewhat weaker. Figure 5 plots, for each protein, the correlation between ω and the various structural quantities versus the correlation between entropy and the same structural quantities. We see that all data points generally fall below the $x = y$ line, and are shifted downwards by approximately 0.1. Thus, correlations of structural quantities with ω are, on average, approximately 0.1 smaller than correlations of the same quantities with entropy.

Besides the measures of buriedness and measures of structural flexibility discussed in the previous subsections, we present in Figure 5 one additional structural quantity, *designed entropy*. Designed entropy is obtained by using computational protein design to generate artificial alignments of designed sequences, and then measuring sequence entropy in these artificial alignments. We had previously shown that designed entropy captures some of the variation observed in natural alignments (Jackson et al., 2013). Here we found that designed entropy performed about as well as the measures of structural flexibility but worse than the measures of buriedness.

Multi-variate analysis of structural predictors

The various structural quantities we have considered are by no means independent of each other. Measures of buriedness co-vary with each other, as do measures of structural flexibility. Further, the latter co-vary with the former, as does designed entropy. To determine the extent to which the various quantities contain independent information about sequence variability, and to assess whether combining multiple structural quantities yields improved predictive power, we carried out a joint multivariate analysis including most of the structural quantities considered in this work. The approach we used is a principal component (PC) regression,

which has previously been used successfully to disentangle genomic predictors of whole-protein evolutionary rates (Drummond et al., 2006; Bloom et al., 2006). In this analysis, we first carry out a principal component analysis of the predictor variables (i.e., the structural quantities such as RSA and RMSF), and we then regress the response (sequence entropy or ω) against the individual components.

Because we wanted to analyze all proteins in our data set individually but in such a way that results were comparable from one protein to the next, we pooled all structural quantities for a single PC analysis and then regressed entropy and ω against each PC separately for each protein. The results of this analysis are shown in Figure 6. The first component (PC1) explained on average the largest amount of variation in sequence entropy (see Figure 6A). We found the second-highest r^2 values, on average, for PC3, while all other components explained very little variation in sequence entropy. When looking at the composition of the components, we found that RSA, iWCN, RMSF, and Var(χ_1) all loaded strongly on PC1, while PC2 and PC3 where primarily represented by designed entropy and B factors (see Figure 6B and C). RMSF also had moderate loadings on PC3. Interestingly, designed entropy and B factors load with equal signs on PC2 but with opposite signs on PC3.

We think that PC1 can be considered as a buriedness component. By definition, PC1 measures the largest amount of variation among the structural quantities, and all structural quantities reflect to some extent the buriedness of residues. PC2 and PC3 are more difficult to interpret. Since designed entropy and B factors load strongly on both but with two different combinations of signs, we think the most parsimonious interpretation is to consider PC2 as a component representing sites with high designed entropy and high spatial fluctuations (as measured by B factors) and PC3 representing sites with high designed entropy and low spatial fluctuations. Using these interpretations, our PC regression analysis suggests that of all the structural quantities, residue buriedness is the best predictor of evolutionary variation. Designed entropy is a useful predictor as well, but it tends to perform better at sites with low spatial fluctuations.

When we included RMSF derived from crystal structures in our analysis, we found comparable results. The main differences occured in PC2 and PC3, where CS RMSF generally loaded in the opposite direction of B factor, and either in the same (PC2) or the opposite (PC3) direction of designed entropy (Figure S1). Finally, results were generally comparable when we considered ω instead of sequence entropy (Figures S2 and S3).

Discussion

We have carried out a comprehensive analysis of how well structural quantities predict evolutionary variation in nine viral proteins. We have found that measures of buriedness generally performed better than measures of structural flexibility. Further, measures of buriedness also performed better than a computational protein-design approach that employed a sophisticated all-atom force field to determine allowed amino-acid distributions at each site. Finally, averaging structural quantities over 15ns of MD simulations provided no improvement in predictive power relative to taking the same quantities from individual crystal structures.

Our results are broadly in agreement with recent work by Echave and collaborators (Yeh et al., 2014; Huang et al., 2014). These authors found that RSA and contact number showed

comparable correlation strengths with evolutionary variation (Yeh et al., 2014). Further, they demonstrated that the observed relationship between evolutionary variation and residue–residue contacts was not consistent with a flexibility model that puts evolutionary variability in proportion to structural flexibility (Huang et al., 2014). Instead, a mechanistic stress model, in which amino-acid substitutions cause physical stress in proportion to the number of residue–residue contacts affected, could explain all the observed data (Huang et al., 2014).

We have found here that correlations between sequence entropy and structural quantities were consistently higher than correlations between the evolutionary-rate ratio ω and structural quantities. This difference likely reflects the distinct physical processes that entropy and ω measure. Entropy is a measure of the amino-acid diversity allowed at a given site. In effect, it reflects how many different amino acids are allowed. By contrast, ω measures how rapidly amino-acid changes occur at a given site. While entropy and ω are generally correlated, a site can have high entropy and comparatively low ω and vice versa. In particular, if mutations rapidly toggle back and forth between two different amino acids at a site, then that site will have high ω and low entropy. By contrast, if a site diversified into a number of different alleles deep in the phylogeny but did not experience much further evolution at later times, then that site will have comparatively high entropy but low ω. Since structural quantities such as measures of buriedness reflect the biophysical constraints imposed on sites, it makes sense that they would be better predictors of the allowed amino-acid diversity at a site than the speed of substitution at that site. By contrast, biological processes such as immune escape would likely be better predictors of substitution rates than amino-acid diversity.

The correlation strengths we observed were consistently lower than those observed in prior work (Jackson et al., 2013; Yeh et al., 2014). We believe that this result was due to our choice of analyzing viral proteins instead of the cellular proteins or enzymes used in prior works. First, while viral sequences are abundant, their alignments may not be as diverged as alignments that can be obtained for sequences from cellular organisms. For example, our influenza sequences spanned only approximately one decade. Despite the high mutation rates observed in RNA viruses, the evolutionary variation that can accumulate over this time span is limited. And the lower the evolutionary divergence, the harder it becomes to resolve differences between more and less conserved sites. Second, many viral proteins experience a substantial amount of selection pressure to evade host immune responses. The resulting positive selection on viral sequences may mask evolutionary constraints imposed by structure. For example, influenza hemagglutinin displays positive selection throughout the entire sequence, and both at buried and at exposed sites (Meyer and Wilke, 2013; Meyer et al., 2013; Suzuki, 2006; Bush et al., 1999).

We found that simple measures of buriedness, such as RSA and contact numbers, were better predictors of evolutionary variation than sequence variability predicted from computational protein design. Thus, simple quantities that can be obtained trivially from PDB structures performed better than a sophisticated protein-design strategy that makes use of an all-atom energy function and requires thousands of CPU-hours to complete. This result highlights that even though computational protein design has yielded impressive results in specific cases (Kuhlman et al., 2003; Röthlisberger et al., 2008; Fleishman et al., 2011), it remains limited in its ability to predict evolutionary variation. We had previously found that flexible backbone design with Rosetta resulted in designs whose surface and core were

too similar (Jackson et al., 2013), and we had suggested that this discrepancy was caused either by the solvation model or the model of backbone flexibility we used (Backrub, see Smith and Kortemme 2008). The results we found here suggest that the model of backbone flexibility may be the cause of at least some of the discrepancies between predicted and observed site variability. In particular, in our PC regression analysis we found that the component in which designed entropy loaded opposite to B factor and MD RMSF generally had the second-highest predictive power for evolutionary variability, after the component representing buriedness. Thus, designed entropy tended to perform better for sites with less structural variability.

Even though RSA and contact number remain the best currently known predictors of evolutionary variation, neither quantity has particularly high predictive power. One reason why predictive power may be low is that neither quantity accounts for correlated substitutions at interacting sites. Yet such correlated substitutions happen regularly. For example, covariation among sites encodes information about residue-residue contacts and 3D structure (Halabi et al., 2009; Burger and van Nimwegen, 2010; Marks et al., 2011; Jones et al., 2014), and evolutionary models that incorporate residue–residue interactions tend to perform better than models that do not (Rodrigue et al., 2005; Bordner and Mittelmann, 2014). An improved predictor of evolutionary variation would have to correctly predict this covariation from structure. In principle, computational protein design, which takes into consideration the atom-level details of the protein structure, should properly reproduce covariation among sites. However, a recent analysis showed that there are significant limitations to the covariation that is predicted (Ollikainen and Kortemme, 2013). In addition, covariation in designed proteins is quite sensitive to the type of backbone variation modeled during design, and improved models of backbone flexibility may be required for improved prediction of covariation among sites (Ollikainen and Kortemme, 2013).

References

Berens P. 2009. CircStat: a MATLAB toolbox for circular statistics. J. Stat. Software 31:1–21.

Bloom J D, Drummond D A, Arnold F H, Wilke C O. 2006. Structural determinants of the rate of protein evolution in yeast. Mol. Biol. Evol. 23:1751–1761.

Bordner A J, Mittelmann H D. 2014. A new formulation of protein evolutionary models that account for structural constraints. Mol. Biol. Evol. 31:736–749.

Burger L, van Nimwegen E. 2010. Disentangling direct from indirect co-evolution of residues in protein alignments. PLoS Comput. Biol. 6:e1000633.

Bush R M, Bender C A, Subbarao K, Cox N J, Fitch W M. 1999. Predicting the evolution of human influenza A. Science 286:1921–1925.

Dean A M, Neuhauser C, Grenier E, Golding G B. 2002. The pattern of amino acid replacements in α/β-barrels. Mol. Biol. Evol. 19:1846–1864.

Drummond D A, Raval A, Wilke C O. 2006. A single determinant dominates the rate of yeast protein evolution. Mol. Biol. Evol. 23:327–337.

Fleishman S J, Whitehead T A, Ekiert D C, Dreyfus C, Corn J E, Strauch E M, Wilson I A, Baker D. 2011. Computational design of proteins targeting the conserved stem region of influenza hemagglutinin. Science 332:816–821.

Franzosa E A, Xia Y. 2009. Structural determinants of protein evolution are context-sensitive at the residue level. Mol. Biol. Evol. 26:2387–2395.

Franzosa E A, Xia Y. 2012. Independent effects of protein core size and expression on residue-level structure-evolution relationships. PLoS ONE 7:e46602.

Goldman N, Thorne J L, Jones D T. 1998. Assessing the impact of secondary structure and solvent accessibility on protein evolution. Genetics 149:445–458.

Goldman N, Yang Z. 1994. A codon-based model of nucleotide substitution for protein-coding DNA sequences. Mol. Biol. Evol. 11:725–736.

Grant B J, Rodrigues A P C, ElSawy K M, McCammon A J, Caves L S D. 2006. Bio3D: an R package for the comparative analysis of protein structures. Bioinformatics 22:2695–2696.

Halabi N, Rivoire O, Leibler S, Ranganathan R. 2009. Protein sectors: Evolutionary units of three-dimensional structure. Cell 138:774–786.

Halle B. 2002. Flexibility and packing in proteins. Proc. Natl. Acad. Sci. USA 99:1274–1279.

Huang T T, del Valle Marcos M L, Hwang J K, Echave J. 2014. A mechanistic stress model of protein evolution accounts for site-specific evolutionary rates and their relationship with packing density and flexibility. BMC Evol. Biol. 14:78.

Jackson E L, Ollikainen N, III A W C, Kortemme T, Wilke C O. 2013. Amino-acid site variability among natural and designed proteins. PeerJ 1:e211.

Jones D T, Buchan D W A, Cozzetto D, Pontil M. 2014. PSICOV: precise structural contact prediction using sparse inverse covariance estimation on large multiple sequence alignments. Mol. Biol. Evol. 31:736–749.

Kabsch W, Sander C. 1983. Dictionary of protein secondary structure: pattern recognition of hydrogen-bonded and geometrical features. Biopolymers 22:2577–2637.

Karplus M, McCammon A. 2002. Molecular dynamics simulations of biomolecules. Nature Struct. Biol. 9:646–652.

Katoh K, Kuma K I, Toh H, Miyata T. 2005. MAFFT version 5: improvement in accuracy of multiple sequence alignment. Nucl. Acids Res. 33:511–518.

Katoh K, Misawa K, Kuma K I, Miyata T. 2002. MAFFT: a novel method for rapid multiple sequence alignment based on fast Fourier transform. Nucl. Acids Res. 30:3059–3066.

Kosakovsky Pond S L, Frost S D W, Muse S V. 2005. HyPhy: hypothesis testing using phylogenetics. Bioinformatics 21:676–679.

Kuhlman B, Dantas G, Ireton G, Gabriele V, Stoddard B. 2003. Design of a novel globular protein fold with atomic-level accuracy. Science 302:1364–1368.

Leaver-Fay A, Tyka M, Lewis S M, Lange O F, Thompson J, Jacak R, Kaufman K, Renfrew D P, Smith C A, Sheffler W, Davis I W, Cooper S, Treuille A, Mandell D J, Richter F, Ban Y E A, Fleishman S J, Corn J E, Kim D E, Lyskov S, Berrondo M, Mentzer S, Popović Z, Havranek J J, Karanicolas J, Das R, Meiler J, Kortemme T, Gray J J, Kuhlman B, Baker D, Bradley P. 2011. ROSETTA3: an object-oriented software suite for the simulation and design of macromolecules. Methods in Enzymology 487:545–574.

Liao H, Yeh W, Chiang D, Jernigan R L, Lustig B. 2005. Protein sequence entropy is closely related to packing density and hydrophobicity. PEDS 18:59–64.

Liu Y, Bahar I. 2012. Sequence evolution correlates with structural dynamics. Mol. Biol. Evol. 29:2253–2263.

Marks D S, Colwell L J, Sheridan R, Hopf T A, Pagnani A, Zecchina R, Sander C. 2011. Protein 3D structure computed from evolutionary sequence variation. PLoS ONE 6:e28766.

Marsh J A, Teichmann S A. 2014. Parallel dynamics and evolution: Protein conformational fluctuations and assembly reflect evolutionary changes in sequence and structure. BioEssays 36:209–218.

Meyer A G, Dawson E T, Wilke C O. 2013. Cross-species comparison of site-specific evolutionary-rate variation in influenza haemagglutinin. Phil. Trans. R. Soc. B 368:20120334.

Meyer A G, Wilke C O. 2013. Integrating sequence variation and protein structure to identify sites under selection. Mol. Biol. Evol. 30:36–44.

Mirny L A, Shakhnovich E I. 1999. Universally conserved positions in protein folds: reading evolutionary signals about stability, folding kinetics and function. J. Mol. Biol. 291:177–196.

Nevin Gerek Z, Kumar S, Banu Ozkan S. 2013. Structural dynamics flexibility informs function and evolution at a proteome scale. Evolutionary Applications 6:423–433.

Ollikainen N, Kortemme T. 2013. Computational protein design quantifies structural constraints on amino acid covariation. PLoS Comput. Biol. 9:e1003313.

Overington J, Donnelly D, Johnson M S, Sali A, Blundell T L. 1992. Environment-specific amino acid substitution tables: tertiary templates and prediction of protein folds. Protein Sci. 1:216–226.

Ramsey D C, Scherrer M P, Zhou T, Wilke C O. 2011. The relationship between relative solvent accessibility and evolutionary rate in protein evolution. Genetics 188:479–488.

Rodrigue N, Lartillot N, Bryant D, Philippe H. 2005. Site interdependence attributed to tertiary structure in amino acid sequence evolution. Gene 347:207–217.

Röthlisberger D, Khersonsky O, Wollacott A M, Jiang L, DeChancie J, Betker J, Gallaher J L, Althoff E A, Zanghellini A, Dym O, Albeck S, Houk K N, Tawfik D S, Baker D. 2008. Kemp elimination catalysts by computational enzyme design. Nature 453:190–195.

Ryckaert J P, Ciccotti G, Berendsen H J C. 1977. Numerical integration of the cartesian equations of motion of a system with constraints: molecular dynamics of n-alkanes. J. Comp. Phys. 23:327–341.

Salomon-Ferrer R, Götz A W, Poole D, Le Grand S, Walker R C. 2013. Routine microsecond molecular dynamics simulations with AMBER on GPUs. 2. Explicit Solvent Particle Mesh Ewald. J. Chem. Theory Comput. 9:3878–3888.

Sanejouand Y H. 2013. Elastic network models: theoretical and empirical foundations. Methods Mol. Biol. 924:601–616.

Scherrer M P, Meyer A G, Wilke C O. 2012. Modeling coding-sequence evolution within the context of residue solvent accessibility. BMC Evol. Biol. Submitted.

Shih C H, Chang C M, Lin Y S, Lo W, Hwang J K. 2012. Evolutionary information hidden in a single protein structure. Proteins: Structure, Function, and Bioinformatics 80:1647–1657.

Smith C A, Kortemme T. 2008. Backrub-like backbone simulation recapitulates natural protein conformational variability and improves mutant side-chain prediction. J. Mol. Biol. 380:742–756.

Spielman S J, Wilke C O. 2013. Membrane environment imposes unique selection pressures on transmembrane domains of G protein-coupled receptors. J. Mol. Evol. 76:172–182.

Stamatakis A. 2006. RAxML-VI-HPC: maximum likelihood-based phylogenetic analyses with thousands of taxa and mixed models. Bioinformatics 22:2688–2690.

Stone E A, Sidow A. 2007. Constructing a meaningful evolutionary average at the phylogenetic center of mass. BMC Bioinformatics 8:222.

Suzuki Y. 2006. Natural selection on the influenza virus genome. Mol. Biol. Evol. 23:1902–1911.

Tien M Z, Meyer A G, Sydykova D K, Spielman S J, Wilke C O. 2013. Maximum allowed solvent accessibilites of residues in proteins. PLOS ONE 8:e80635.

Wilke C O, Drummond D A. 2010. Signatures of protein biophysics in coding sequence evolution. Cur. Opin. Struct. Biol. 20:385–389.

Yang Z. 2000. Maximum likelihood estimation on large phylogenies and analysis of adaptive evolution in human influenza virus A. J. Mol. Evol. 51:423–432.

Yeh S W, Liu J W, Yu S H, Shih C H, Hwang J K, Echave J. 2014. Site-specific structural constraints on protein sequence evolutionary divergence: Local packing density versus solvent exposure. Mol. Biol. Evol. 31:135–139.

Tables

Table 1: **PDB structures considered in this study.**

Viral Protein	PDB ID	Chain	Sequence Length	Number of Sequences
Hemagglutinin Precursor	1RD8	AB	503	1039
Dengue Protease Helicase	2JLY	A	451	2362
West Nile Protease	2FP7	B	147	237
Japanese Encephalitis Helicase	2Z83	A	426	145
Hepatitis C Protease	3GOL	A	557	1021
Rift Valley Fever Nucleoprotein	3LYF	A	244	95
Crimean Congo Nucleocapsid	4AQF	B	474	69
Marburg RNA Binding Domain	4GHA	A	122	42
Influenza Nucleoprotein	4IRY	A	404	943

Table 2: **Availability of homologous crystal structures.** Even though most viral proteins have many PDB structures available, the sequence divergence among these structures is low. To calculate RMSF from crystal structures, we here considered all proteins for which we could find at least five homologous structures at 5% pairwise sequence divergence (highlighted in bold).

Viral Protein	BLAST hits[a]	Unique sequences			
		all	$\geq 2\%$[b]	$\geq 5\%$[b]	$\geq 10\%$[b]
Hemagglutinin Precursor	63	17	10	**9**	7
Dengue Protease Helicase	31	13	7	**7**	7
West Nile Protease	21	16	10	**7**	6
Japanese Encephalitis Helicase	31	12	7	**7**	7
Hepatitis C Protease	302	33	10	**5**	4
Rift Valley Fever Nucleoprotein	95	9	5	**5**	5
Crimean Congo Nucleocapsid	7	4	3	2	2
Marburg RNA Binding Domain	63	9	5	3	3
Influenza Nucleoprotein	69	15	4	4	2

[a] BLAST hits against all sequences in the PDB, excluding hits with $< 35\%$ sequence identity and $< 90\%$ alignment length
[b] Unique sequences at indicated minimum pairwise sequence divergence

Table 3: **Correlations between quantities obtained from MD trajectories and from crystal structures.** For each quantity and each protein, we calculated the Spearman correlation ρ between the values obtained from MD time averages and the values obtained from crystal structures. We then calculated the minimum, maximum, mean, and standard deviation of these correlations.

| Quantity	min ρ	max ρ	$\langle\rho\rangle$	SD(ρ)
RSA	0.937	0.981	0.948	0.012
CN	0.964	0.993	0.976	0.008
WCN	0.973	0.991	0.984	0.006
RMSF	0.218	0.723	0.502	0.181

Figures
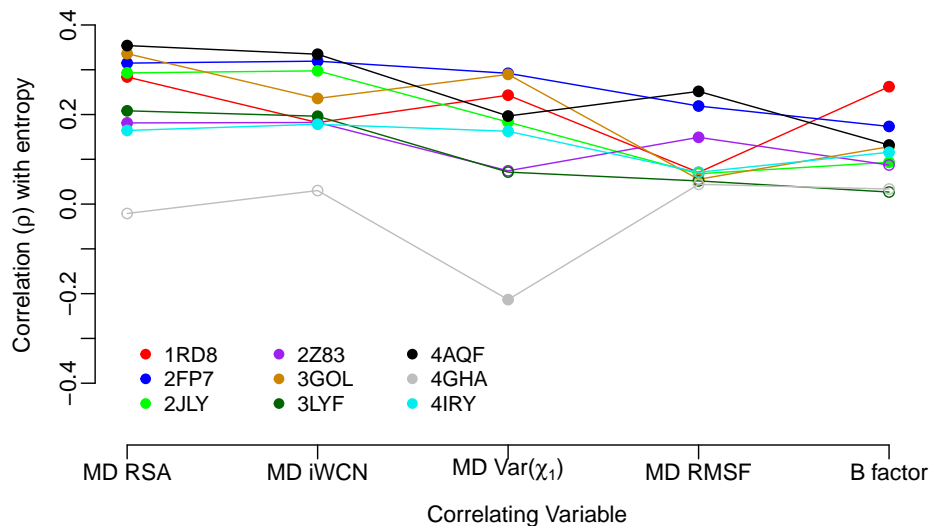
Figure 1: **Spearman correlation of sequence entropy with measures of buriedness and of structural variability.** Each symbol represents one correlation coefficient for one protein structure. Significant correlations ($P < 0.05$) are shown as filled symbols, and insignificant correlations ($P \leq 0.05$) are shown as open symbols. The quantities RSA, iWCN, $\mathrm{Var}(\chi_1)$, and RMSF were obtained as time-averages over 15ns of MD simulations. B factors were obtained from crystal structures. Compared to the measures of structural variability, the buriedness measures consistently show stronger correlations with sequence entropy.
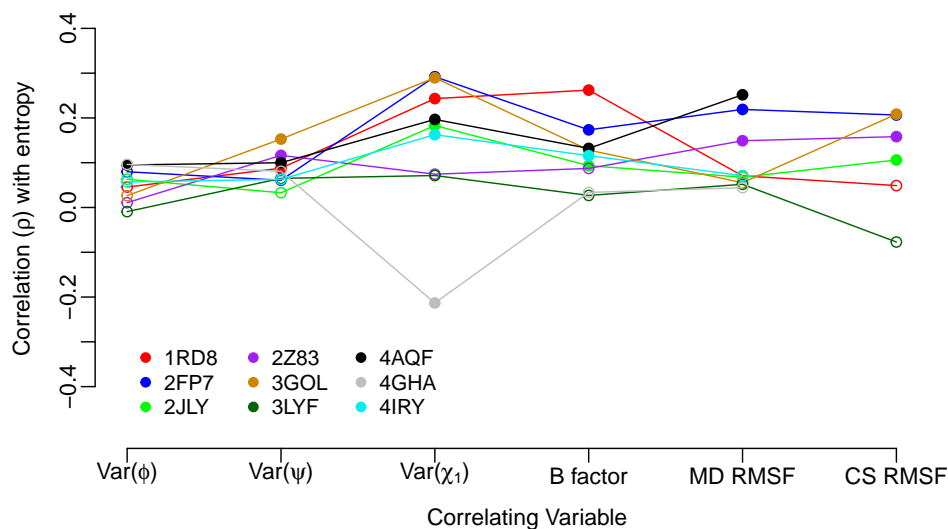
Figure 2: **Spearman correlation of sequence entropy with measures of structural variability.** Each symbol represents one correlation coefficient for one protein structure. Significant correlations ($P < 0.05$) are shown as filled symbols, and insignificant correlations ($P \leq 0.05$) are shown as open symbols. The quantities $\text{Var}(\psi)$, $\text{Var}(\phi)$, $\text{Var}(\chi_1)$, and MD RMSF were obtained as time-averages over 15ns of MD simulations. B factors were obtained from crystal structures. CS RMSF values were obtained from alignments of homologous crystal structures. Almost all structural measures of variability correlate weakly but significantly with sequence entropy.
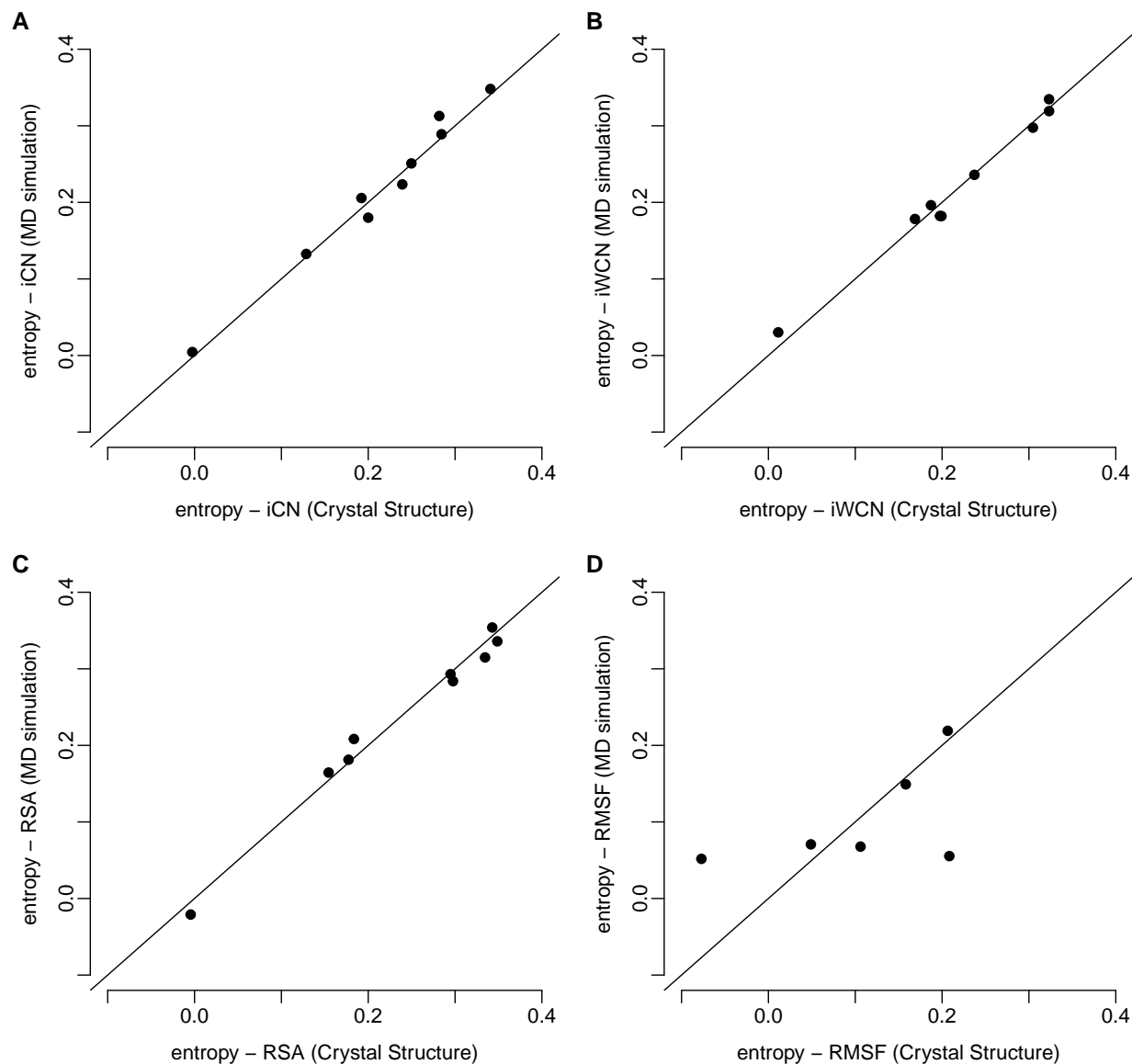
Figure 3: **Spearman correlations of sequence entropy with MD-derived and crystal-structure derived structural measures.** The vertical axes in all plots represent the Spearman correlation of sequence entropy with one structural variable obtained from $15ns$ of Molecular Dynamics (MD) simulations. The horizontal axes represent the Spearman's rank correlation coefficient of sequence entropy with the same structural variable as in the vertical axes but measured from protein crystal structures. Each dot represents one correlation coefficient for one protein structure. The quantities iCN, iWCN, and RSA have nearly identical predictive power for sequence entropy regardless of whether they are derived from MD simulations or from crystal structures. By contrast, RMSF from MD simulations leads to very different correlations than RMSF from crystal structures does.
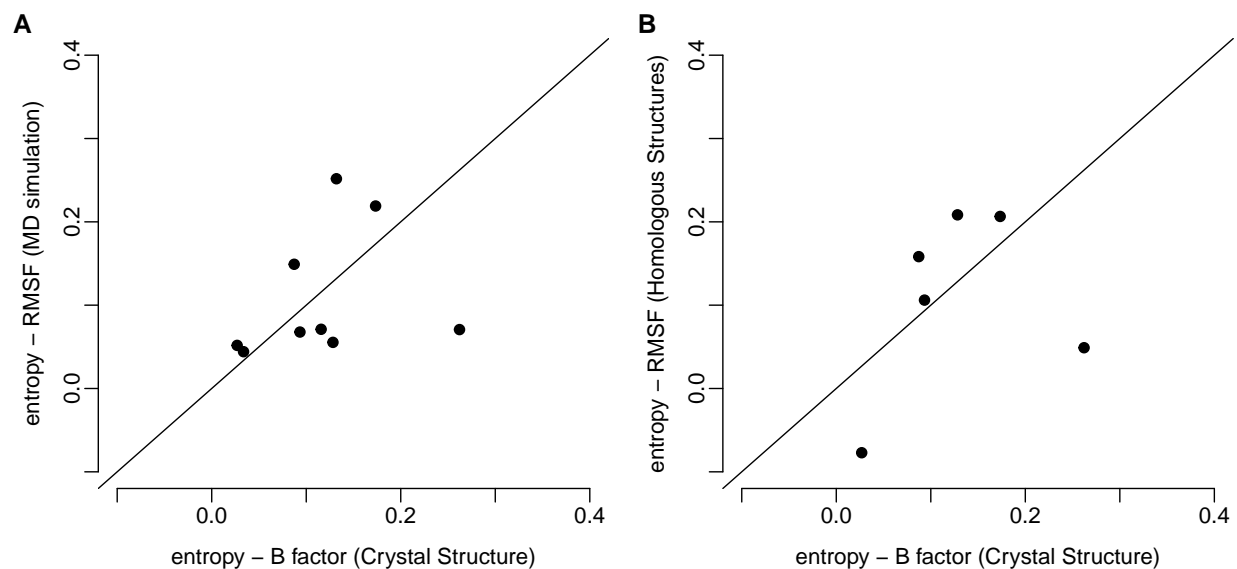
Figure 4: **Spearman correlations of sequence entropy with measures of structural variability.** Vertical and horizonal axes represent Spearman correlations of the indicated quantities. Each dot represents one correlation coefficient for one protein structure. MD RMSF, crystal-structure RMSF, and B factors all have explain different amounts of variance in sequence entropy for different proteins.
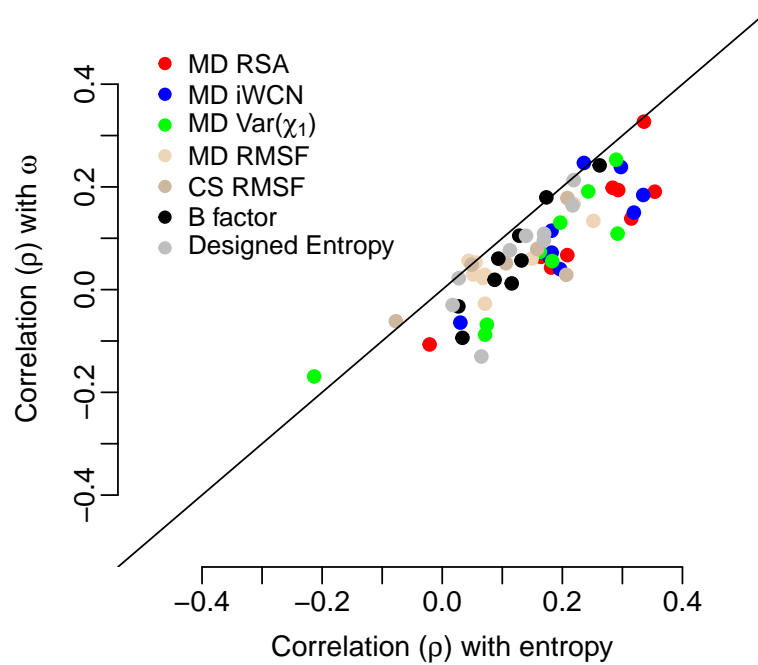
Figure 5: **Spearman correlations of structural quantities with sequence entropy and with the evolutionary rate ratio** ω**.** All structural quantities generally predict as much as or more variation in sequence entropy than in ω.
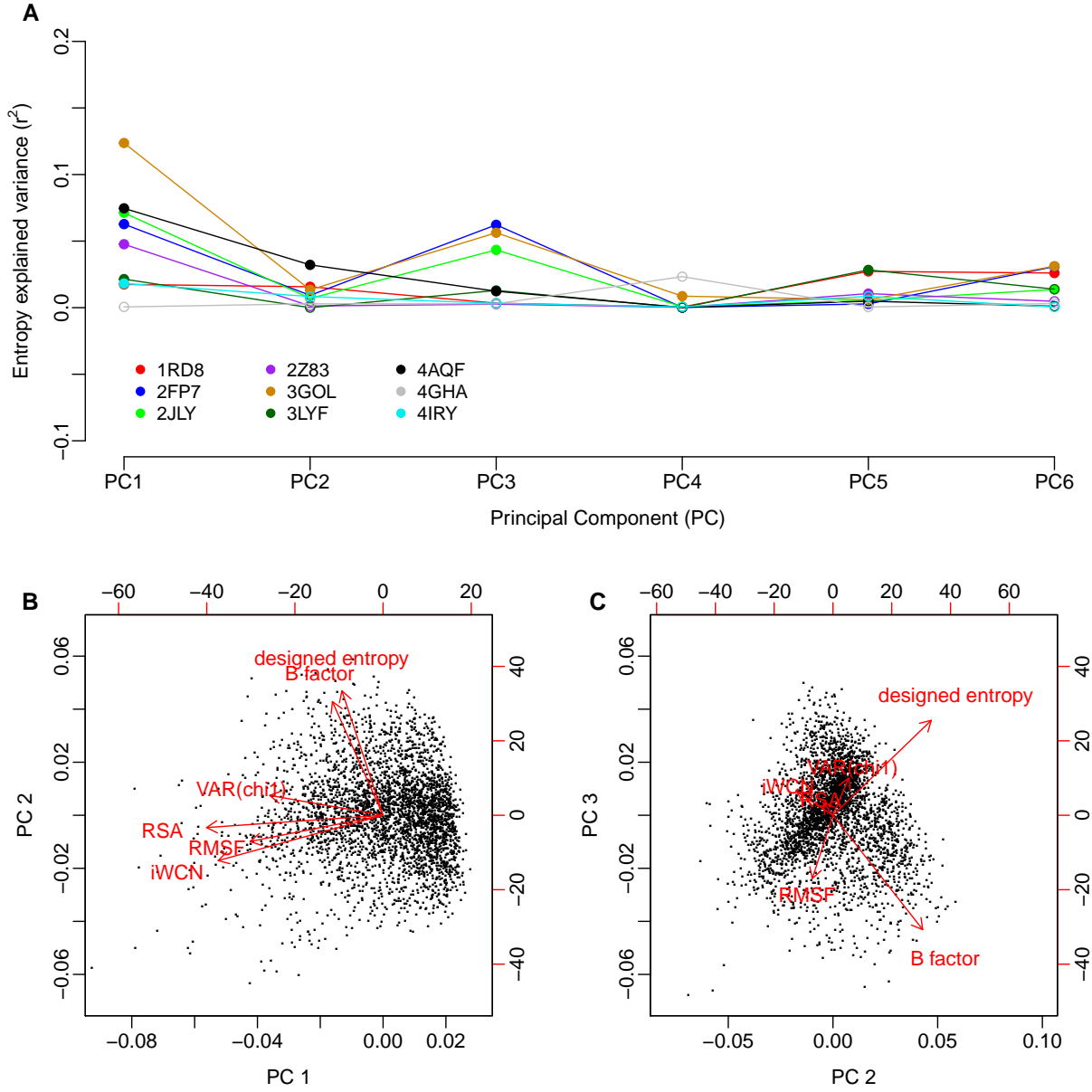
Figure 6: **Principal Component (PC) Regression of sequence entropy against the structural variables.** **(A)** Variance in entropy explained by each principal component. For most proteins, PC1 and PC3 show the strongest correlations with sequence entropy. Significant correlations ($P < 0.05$) are shown as filled symbols, and insignificant correlations ($P \leq 0.05$) are shown as open symbols. **(B)** and **(C)** Composition of the three leading components. Red arrows represent the loadings of each of the structural variables on the principal components; black dots represent the amino acid sites in the PC coordinate system. The variables RSA, iWCN, MD RMSF, and $\mathrm{Var}(\chi_1)$ load strongly on PC1 and weakly on PC2, while B factor and designed entropy load strongly on PC2 and weakly on PC1. Interestingly, B factor and designed entropy also load strongly on PC3, but in opposite directions.
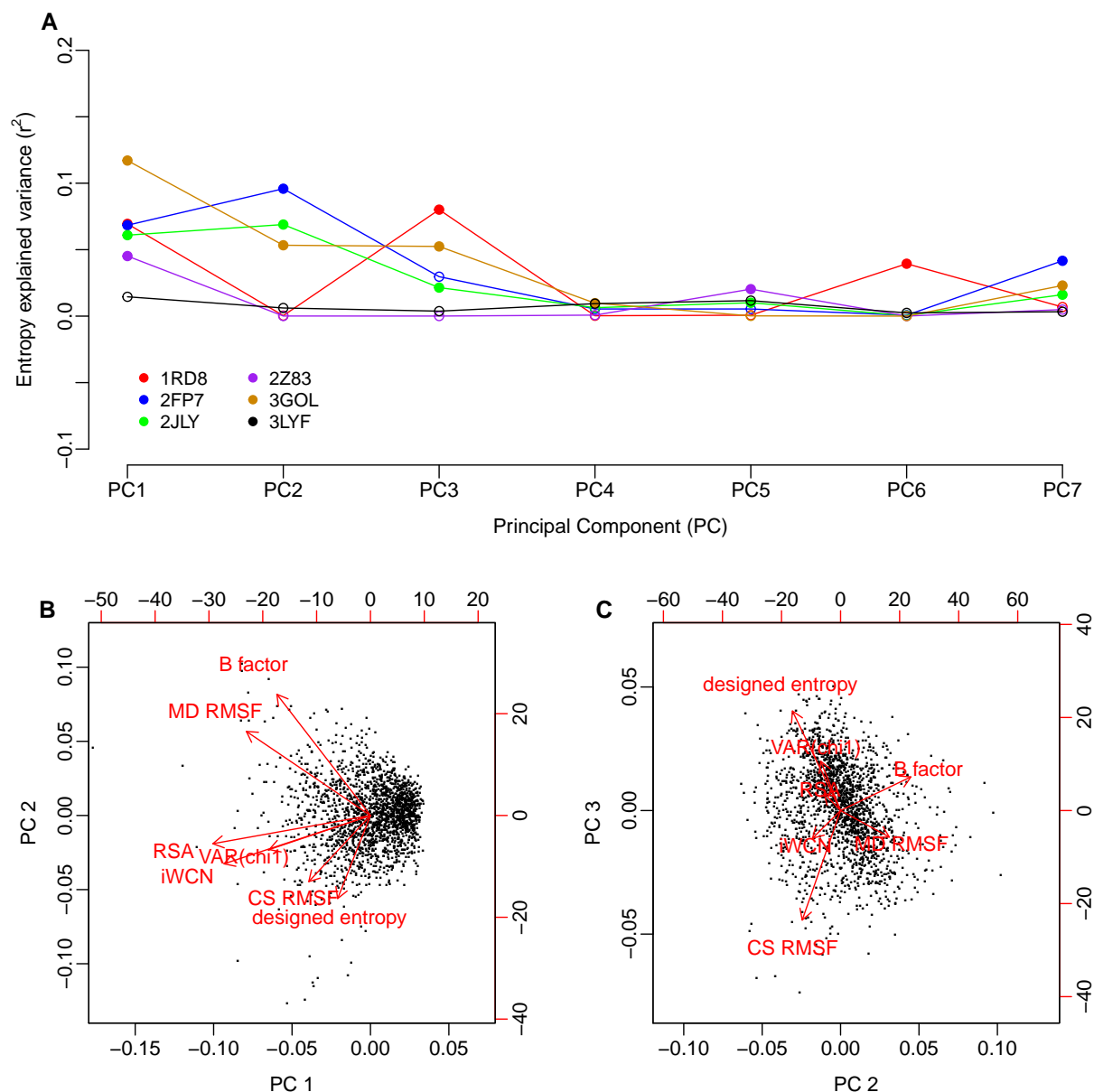
Supplementary Figures

Figure S1: **Principal Component (PC) Regression of sequence entropy against the structural variables, including CS RMSF. (A)** Variance in entropy explained by each principal component. For most proteins, PC1 and either PC2 or PC3 show the strongest correlations with sequence entropy. Significant correlations ($P < 0.05$) are shown as filled symbols, and insignificant correlations ($P \leq 0.05$) are shown as open symbols. **(B)** and **(C)** Composition of the three leading components. Red arrows represent the loadings of each of the structural variables on the principal components; black dots represent the amino acid sites in the PC coordinate system.
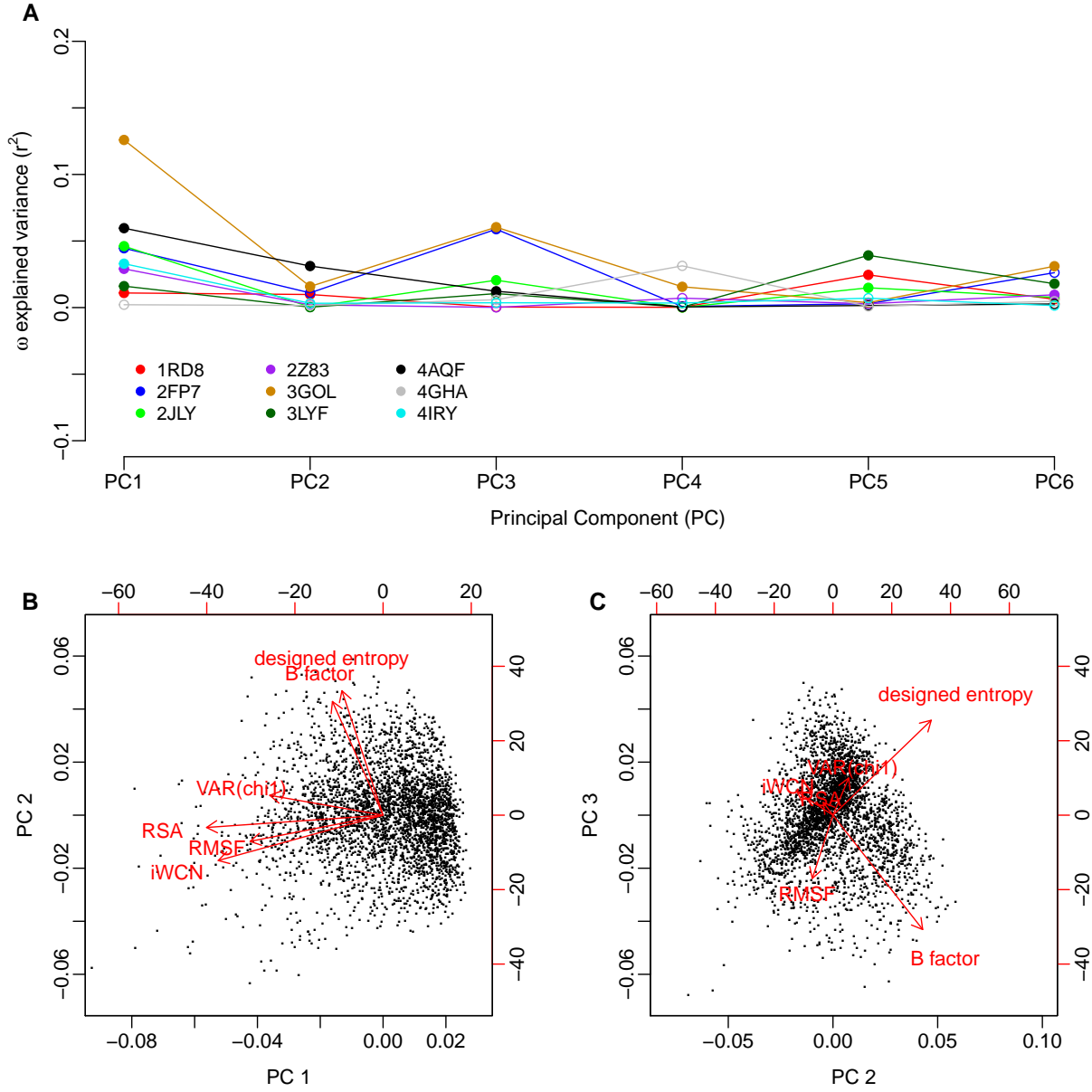
Figure S2: **Principal Component (PC) Regression of ω against the structural variables.** **(A)** Variance in ω explained by each principal component. For most proteins, PC1 and PC3 show the strongest correlations with ω. Significant correlations ($P < 0.05$) are shown as filled symbols, and insignificant correlations ($P \leq 0.05$) are shown as open symbols. **(B)** and **(C)** Composition of the three leading components. Red arrows represent the loadings of each of the structural variables on the principal components; black dots represent the amino acid sites in the PC coordinate system. Note that parts B and C are identical to those shown in Figure 6.
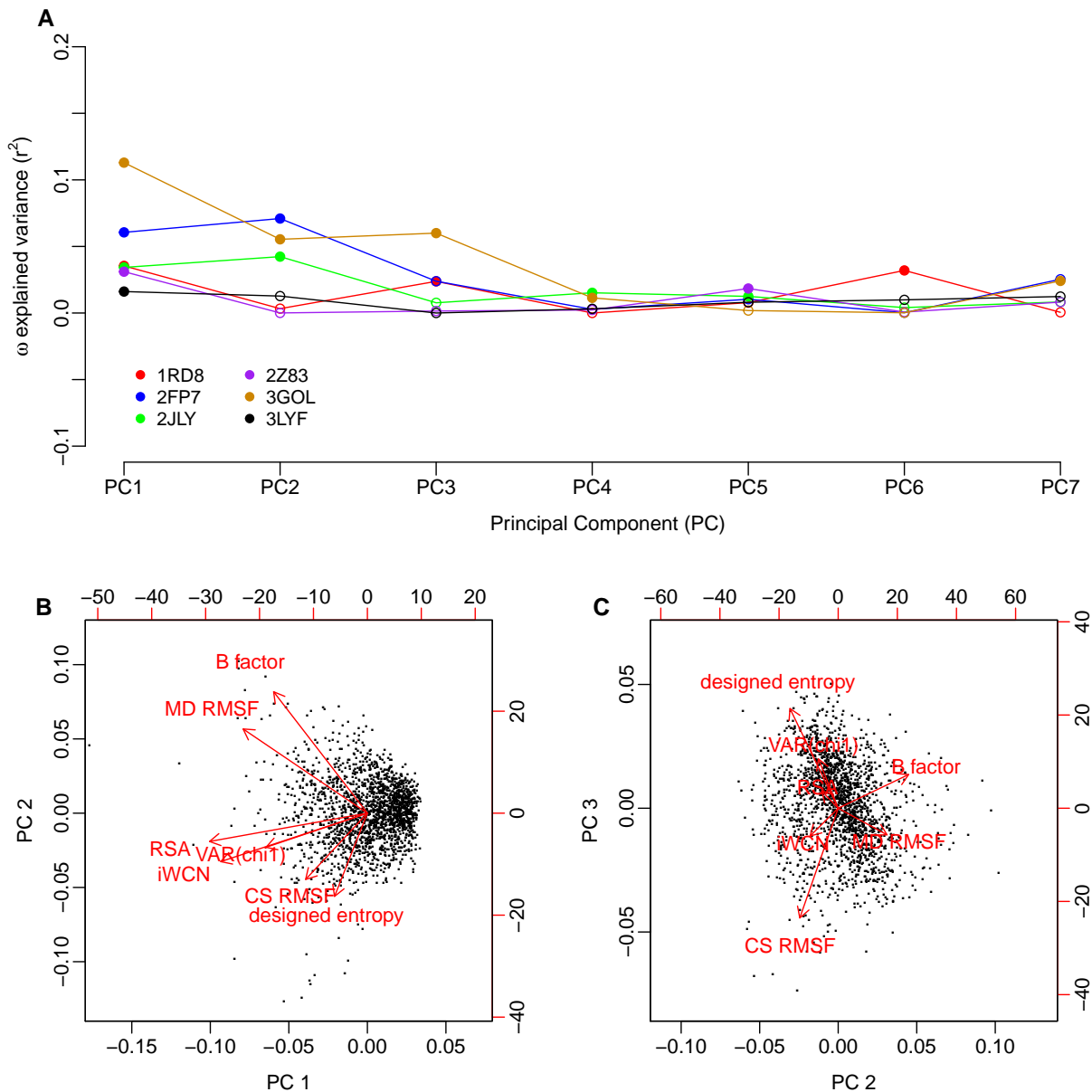
Figure S3: **Principal Component (PC) Regression of ω against the structural variables, including CS RMSF. (A)** Variance in ω explained by each principal component. For most proteins, PC1 and either PC2 or PC3 show the strongest correlations with ω. Significant correlations ($P < 0.05$) are shown as filled symbols, and insignificant correlations ($P \leq 0.05$) are shown as open symbols. **(B)** and **(C)** Composition of the three leading components. Red arrows represent the loadings of each of the structural variables on the principal components; black dots represent the amino acid sites in the PC coordinate system. Note that parts B and C are identical to those shown in Figure S1.